Supplement of Biogeosciences, 22, 5231–5246, 2025
https://doi.org/10.5194/bg-22-5231-2025-supplement

Biogeosciences Open Access EGU

Supplement of

Drivers of and uncertainty in Amazon carbon sink long-term and inter-annual variability in CMIP6 models

Matteo Mastropierro et al.

Correspondence to: Matteo Mastropierro (matteo.mastropierro@unive.it)

Table S1: Overview of ESMs considered in this study

ESM	Ref	Curvilinear Ocean Grid	Land carbon	N cycle	P cycle	Fires	Dynamic vegetation	ECS (°C)
IPSL-CM6A-LR	(Boucher et al., 2020)	Yes	ORCHIDEE, br.2.0	No	No	No	No	4.70
CNRM-ESM2-1	(Séférian et al., 2019)	Yes	ISBA-CTRIP	Implicit	No	Yes (natural)	No	4.79
CanESM5	(Swart et al., 2019)	Yes	CLASS-CTEM	Implicit	No	No	dynamic wetlands	5.64
UKESM1-0-LL	(Sellar et al., 2019)	No	JULES-ES-1.0	Yes	No	No	Yes	5.36
MIROC-ES2L	(Hajima et al., 2020)	No	VISIT-e	Yes	No	No	No	2.66
ACCESS-ESM1-5	(Ziehn et al., 2020)	No	CABLE	Yes	Yes	No	No	3.88
MPI-ESM1-2-LR	(Mauritsen et al., 2019)	Yes	JSBACH3.2	Yes	No	No	Yes	3.03
NorESM2-LM	(Seland et al., 2020)	No	CLM5	Yes	No	Yes	No	2.49
CMCC-ESM2	(Lovato et al., 2022)	Yes	CLM-4.5	Yes	No	Yes (natural)	No	3.58
CESM2	(Danabasoglu et al., 2020)	No	CLM5	Yes	No	Yes	dynamic wetlands	4.68
MRI-ESM2-0	(Yukimoto et al., 2019)	No	HAL	No	No	No	No	3.14

Earth System Models evaluation

The ESM ability to simulate ENSO is first assessed in terms of the Nino3.4 index seasonality (phase-locking, Figure S1). Figure S1 clearly shows that all the models, with the exception of CanESM5 and ACCESS-ESM1-5, exhibit a stronger interannual variability than observations, represented by the HadISST dataset (Rayner et al., 2003), during all the calendar months (black line). Those two models, on the opposite, are characterized by a lower seasonality of the ENSO signal, with higher and lower than observed variability during boreal summer and boreal winter months, respectively. Beyond the bias in the annual standard deviation, the normalized index indicates that ESMs typically yield a much higher minimum from March to August and lower maximum from September to January compared to observations (Figure S1b), thus displaying a negative bias in the amplitude of ENSO seasonal variations.

We also considered the ability of the ESMs to simulate the climatology of the Amazon basin as well as its land carbon and surface energy fluxes by assessing their seasonality. A dry precipitation bias is persistent during the whole year and for all the ESMs (Ortega *et al.*, 2021; Monteverde *et al.*, 2022, Figure S2, panel a), with the only partial exception of ACCESS-ESM1-5 and MRI-ESM2-0. Despite this, however, not all the models display a consistent dry bias for soil moisture, but rather roughly half of them overestimate the volumetric soil content of water, most likely a direct consequence of the parameterization of soil water depth in the different land models used (Qiao *et al.*, 2022, Figure S2, panel c). Temperatures are also overestimated in the Amazon basin, both concerning their seasonal amplitude cycle, which is accentuated in ESM, as well as considering monthly mean values, which are sensibly higher during the whole calendar year, compared to ERA5 reanalysis (Figure S2, panel b). Considering the energy fluxes, shortwave incoming radiation is probably the most consistent bias observable in the region considered (Figure S3, panel d), and its presence has strongly persisted since the 5th generation of CMIP models (Wild et al., 2015). Despite a correct seasonality, the values of incoming radiation are almost two times the FLUXCOM ones (Jung et al., 2019), used as a validation reference: this bias is a consequence of low cloudiness within the tropical basin, and most likely it is the direct factor that generates the dry precipitation bias. ESMs also struggle to reproduce the seasonal cycle of GPP, TER and consequently NEP (Figure S3, panel , b and c), as well as the yearly mean values of the carbon fluxes (Figure S4). First, the general behaviour of the ESMs is a shift in the lower photosynthetic productivity peak towards the end of the year (Figure S3 panel b). Regarding NEP, all the models depict a clear and strong underestimation of boreal spring, autumn and winter values, compared to the FLUXOM carbon fluxes dataset (Jung et al., 2020), as clear in Figure S3c. The NEP bias is related to a combination of TER overestimation and an underestimation of GPP, or both (MRI-ESM2-0, MPI-ESM1-2-LR and UKESM1-0-LL, Figure S3). Specifically, the high GPP and TER displayed by those three models compared to FLUXCOM and the other ESMs indicates a particularly high vegetation (and thus Land Module) sensitivity to climatological forcings.

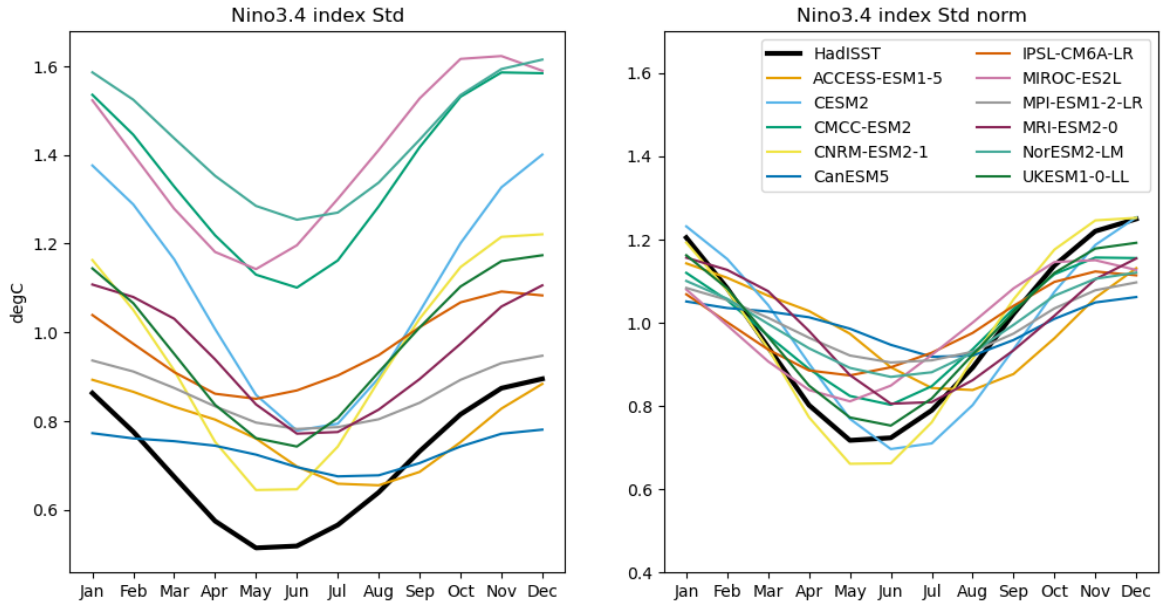

Figure S1: Model biases with respect to the HadISST dataset in ENSO seasonal variability, for the period 1979/2013. a) seasonality as expressed by the Nino3.4 index standard deviation, b) seasonality expressed by the normalized Nino3.4 standard deviation.

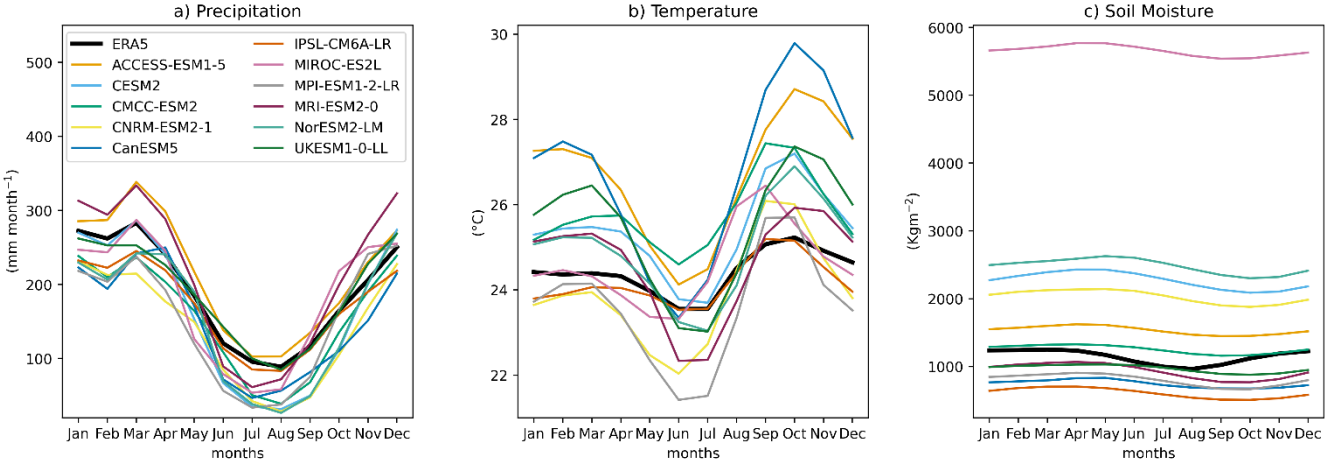

Figure S2: Model biases with respect to the ERA5 dataset in the climatological seasonal variability, for the period 1979/2013. Shown are the monthly zonal means within the Amazon basin for a) precipitation, b) temperature and c) soil moisture.

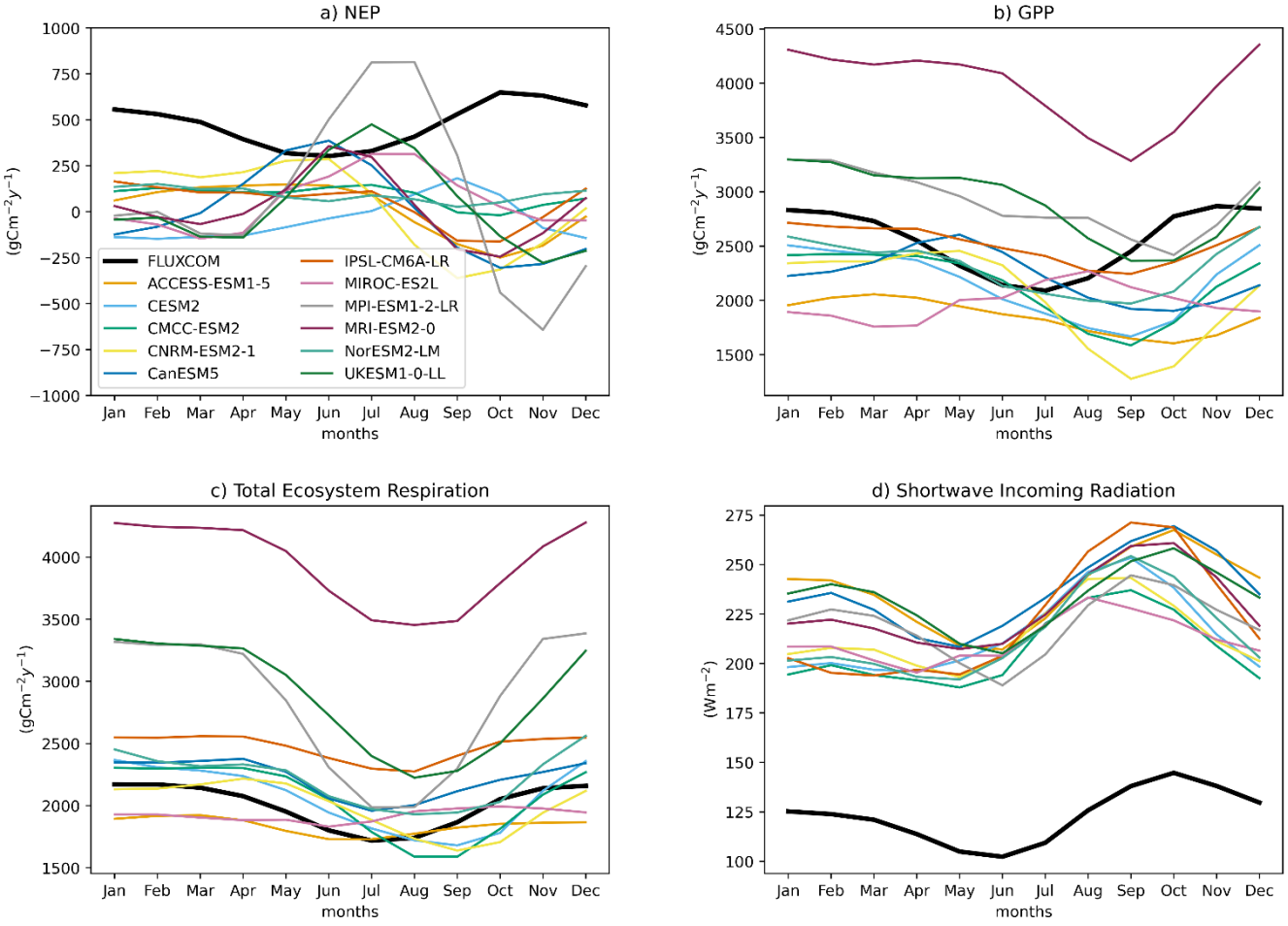

Figure S3: Model biases with respect to the FLUXCOM dataset in the seasonal variability, for the period 1979/2013. Shown are the monthly zonal means within the Amazon basin for a) NEP, b) GPP and c) TER and d) shortwave incoming radiation.

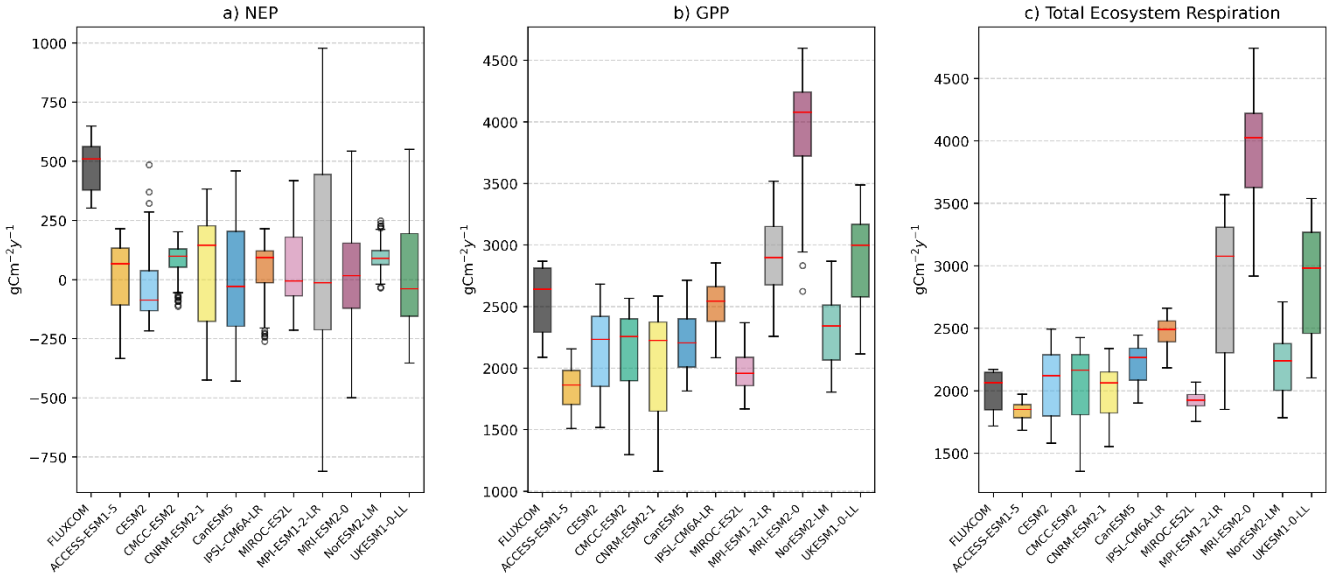

Figure S4: Model biases with respect to the FLUXCOM dataset in the distribution of carbon fluxes values, for the period 1979/2013. Shown are the yearly zonal values within the Amazon basin for a) NEP, b) GPP and c) total ecosystem respiration (TER, the sum of autotrophic and heterotrophic respirations for ESMs).

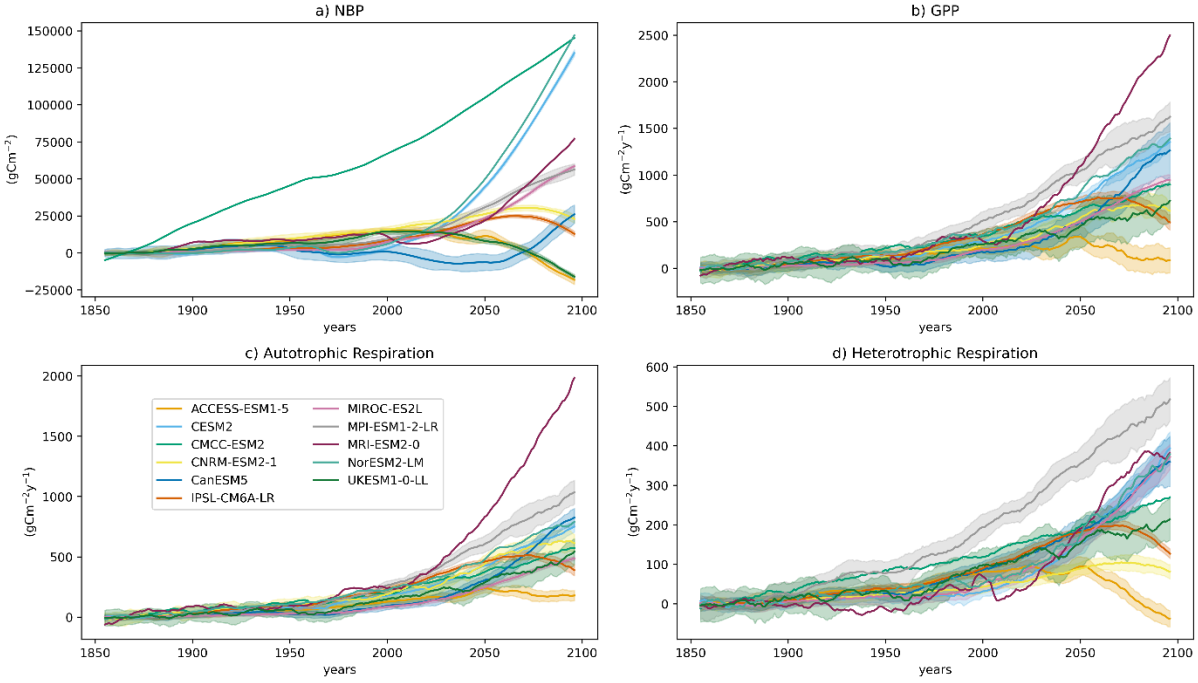

Figure S5: Simulated anomalies of (a) cumulative NBP, (b) GPP, (c) Ra and (d) Rh in the Amazon basin for the historical and ssp585 experiments. Trends are computed with respect to the 1850 mean and are visualized as a 10-years moving average for clarity. For the models with more than one realization, both the model-ensemble mean (line) and the spread (±1 standard deviation, shading) are shown.

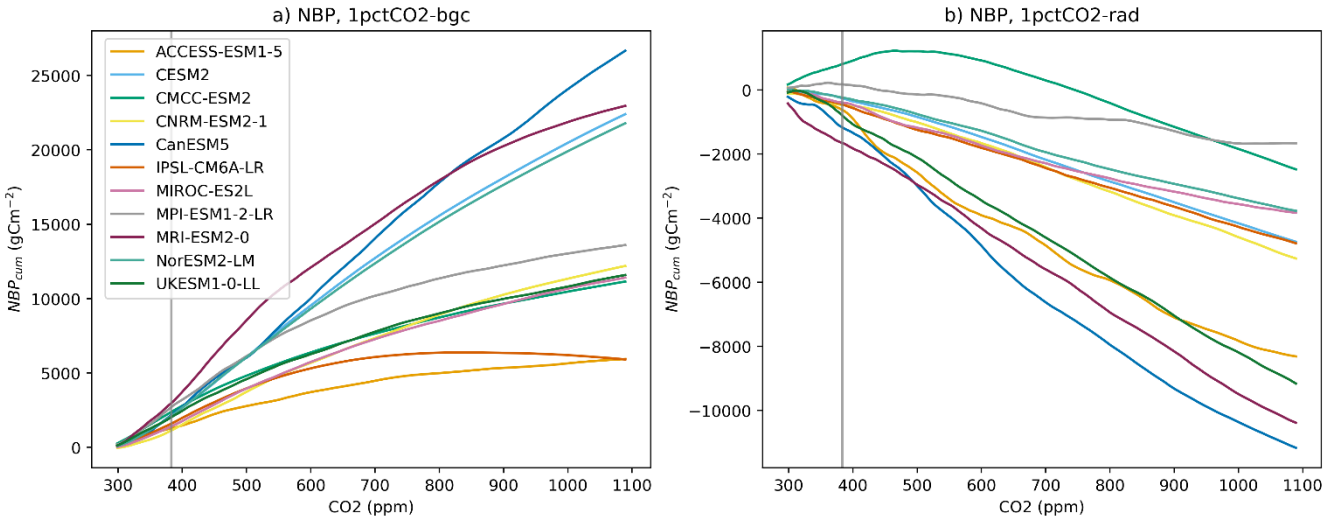

Figure S6: Cumulative NBP anomalies from a) 1pctCO2-bgc and b) 1pctCO2-rad simulations. Trends are computed with respect to the start of the simulation and are showed as 10-years moving averages for clarity.

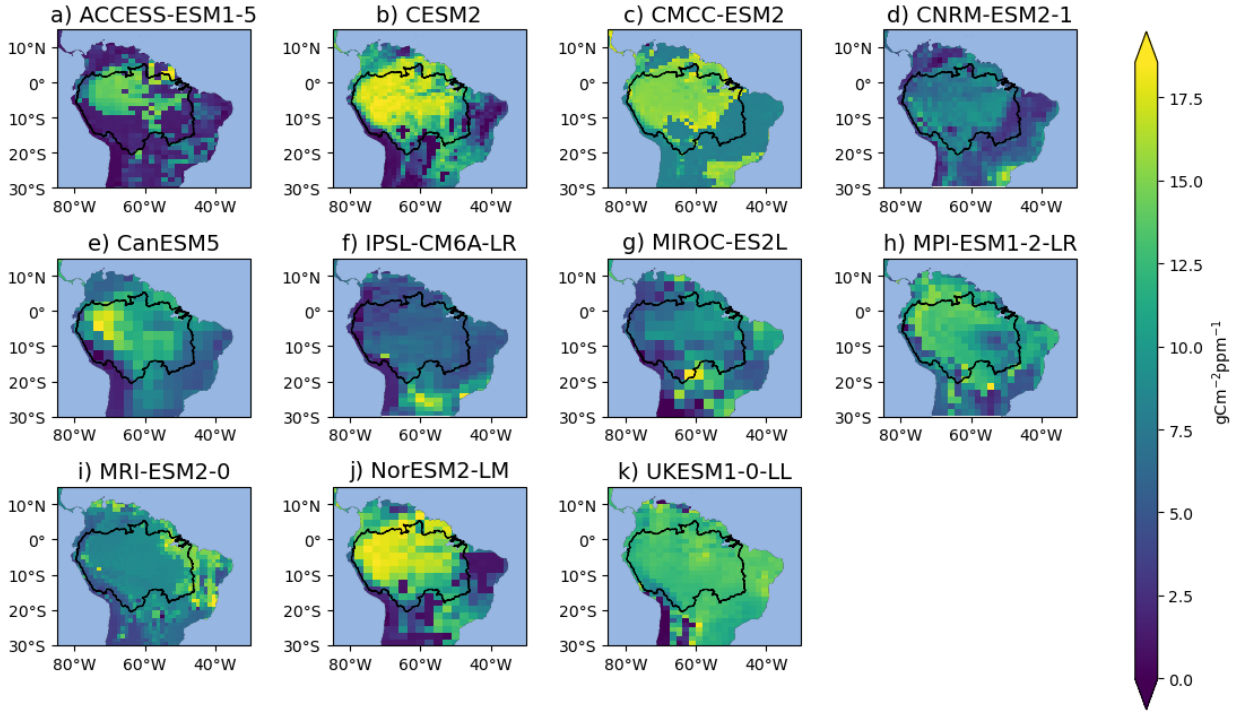

Figure S7: Estimates of the carbon-concentration feedback (β) for the ESMs considered. The Amazon basin, obtained from the SO HYBAM service (https://hybam.obs-mip.fr/), is also represented.

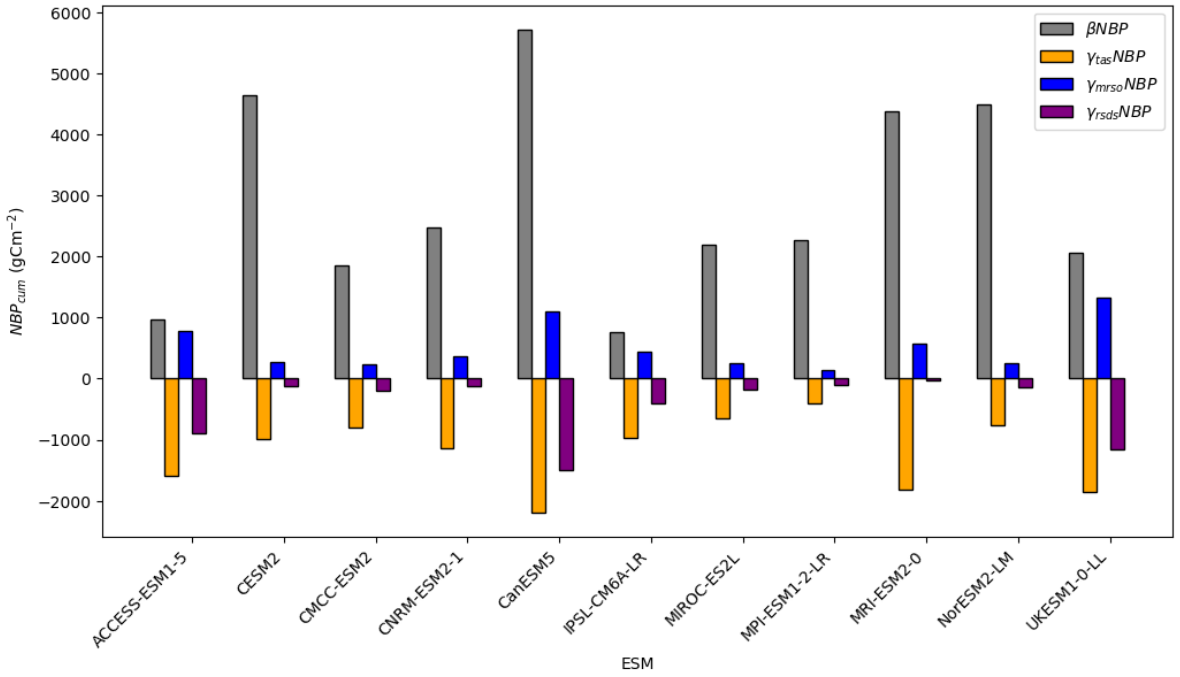

Figure S8: Standardized values of β and γ averaged over the Amazon basin, representing their contribution to cumulative NBP in the 1pctCO2-bgc and 1pctCO2-rad simulations respectively.

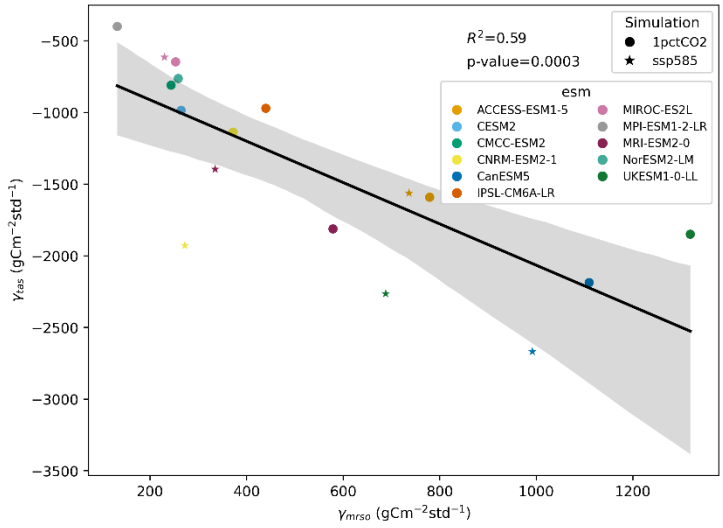

Figure S9: Inverse relationship between ESMs representation of temperature (γ_{tas}) and soil moisture (γ_{mrso}) impacts in 1pctCO2-rad and ssp585-rad simulations.

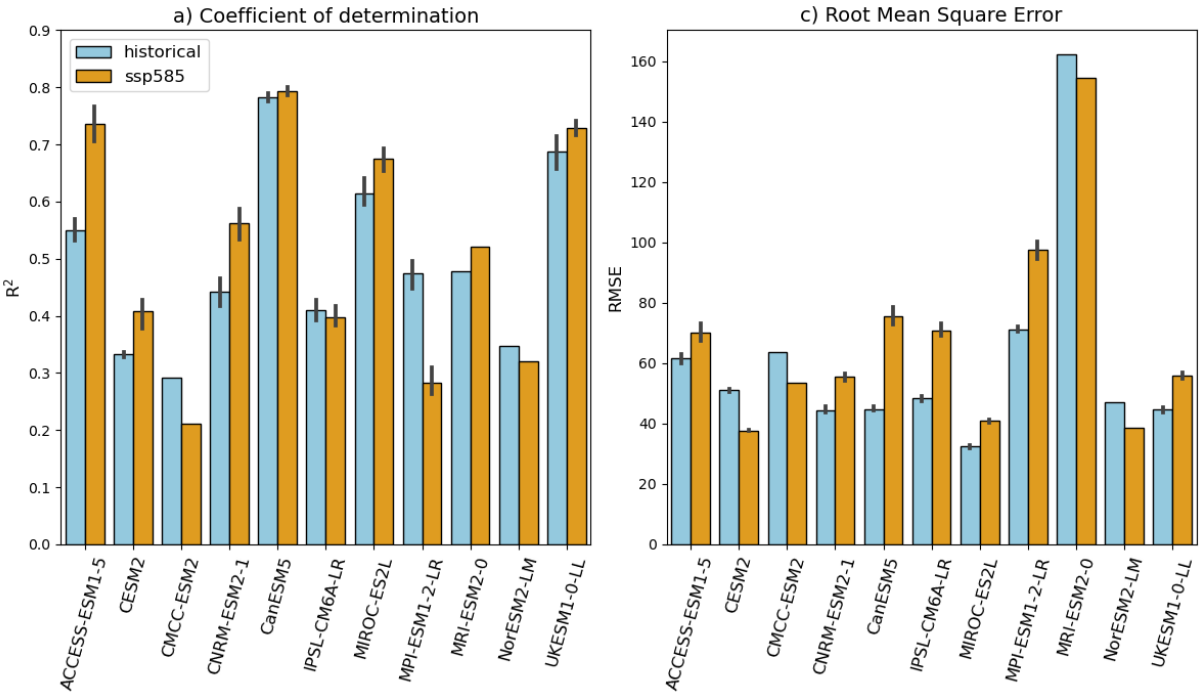

Figure S10: Predictive skills of the ridge regression model by adopting the 5-fold cross-validation procedure, for every ESM and for both the historical and the ssp585 scenario. In panel a) is reported R^2, in panel b) the RMSE.

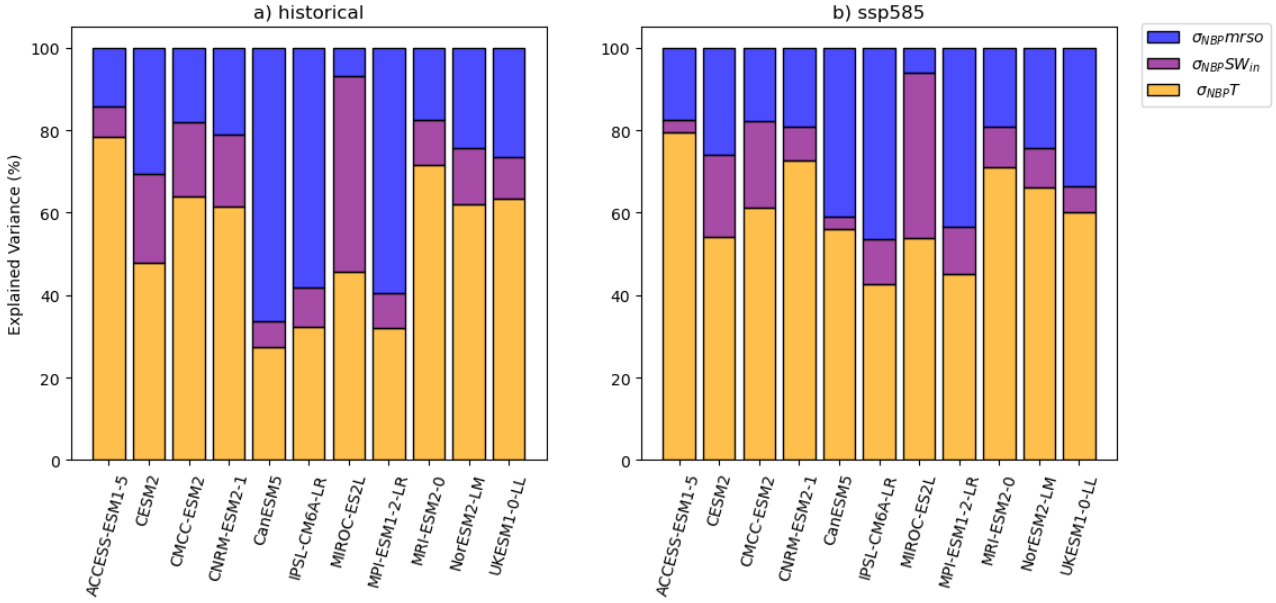

Figure S11: Share of interannual NBP explained variance (%), by means of temperature (yellow), soil-moisture (blue) and shortwave incoming radiation (purple) for every ESM for a) historical period and b) ssp585 scenario.

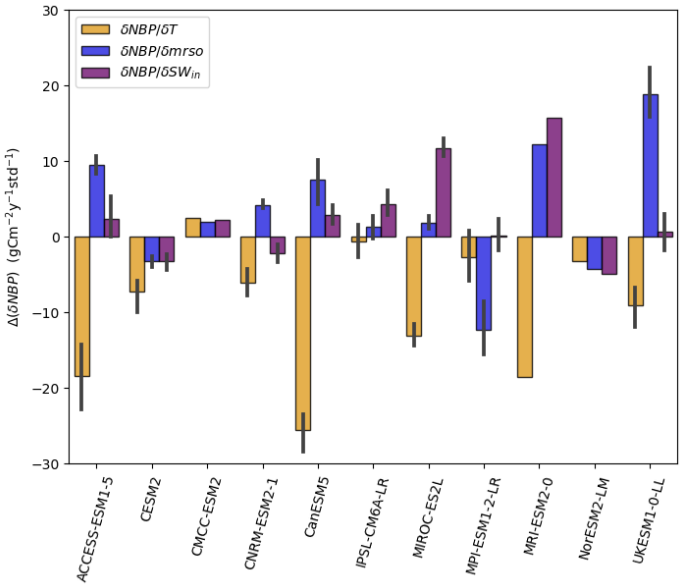

Figure S12: Changes in the coefficients of the 5-fold CV ridge regression model in the ssp585 scenario with respect to the historical period, for all the ESMs. Shown are the Amazon basin mean values of the regression coefficients.

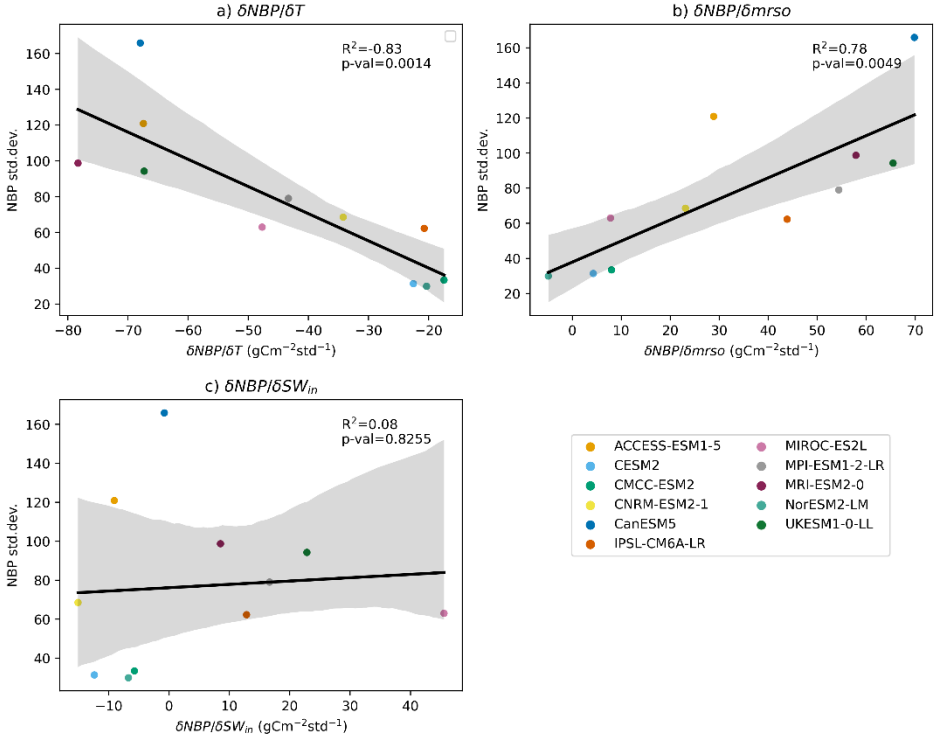

Figure S13: Intermodel uncertainty in interannual variability of NBP (y-axis) as explained by the 5-fold CV ridge regression coefficients with respect to: a) temperature, b) soil moisture and c) shortwave incoming radiation.

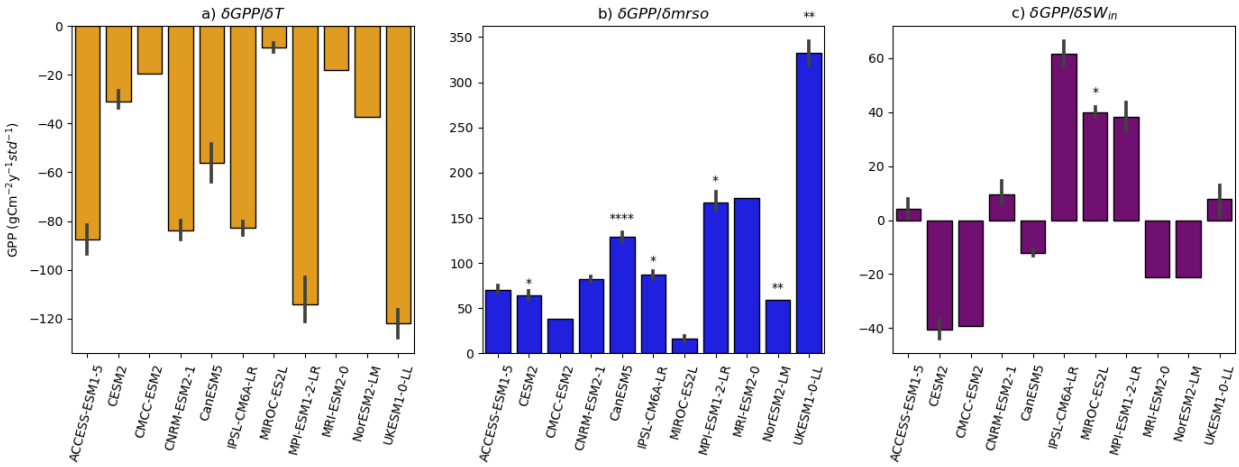

Figure S14: Partial derivatives explaining the contribution of temperature (a), soil moisture (b) and shortwave incoming radiation (c) to interannual GPP, averaged across the Amazon basin. The black vertical bars represent the spread in the predictors coefficients for models with more than one realization available, whereas the stars indicate the level of significance (p-value), averaged over the Amazon basin, associated to every coefficient. Statistical significance refers to the following convention: *: 1.00e-02 < p <= 5.00e-02; **: 1.00e-03 < p <= 1.00e-02; ***: 1.00e-04 < p <= 1.00e-03; ****: p <= 1.00e-04.

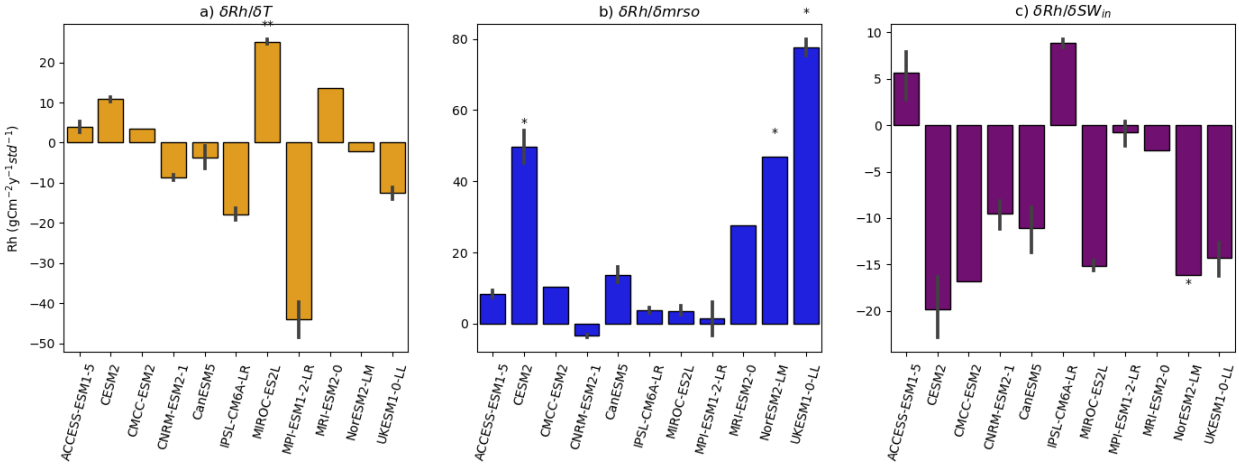

Figure S15: Partial derivatives explaining the contribution of temperature (a), soil moisture (b) and shortwave incoming radiation (c) to interannual Rh, averaged across the Amazon basin. The black vertical bars represent the spread in the predictors coefficients for models with more than one realization available, whereas the stars indicate the level of significance (p-value), averaged over the Amazon basin, associated to every coefficient. Statistical significance refers to the following convention: *: 1.00e-02 < p <= 5.00e-02; **: 1.00e-03 < p <= 1.00e-02; ***: 1.00e-04 < p <= 1.00e-03; ****: p <= 1.00e-04.

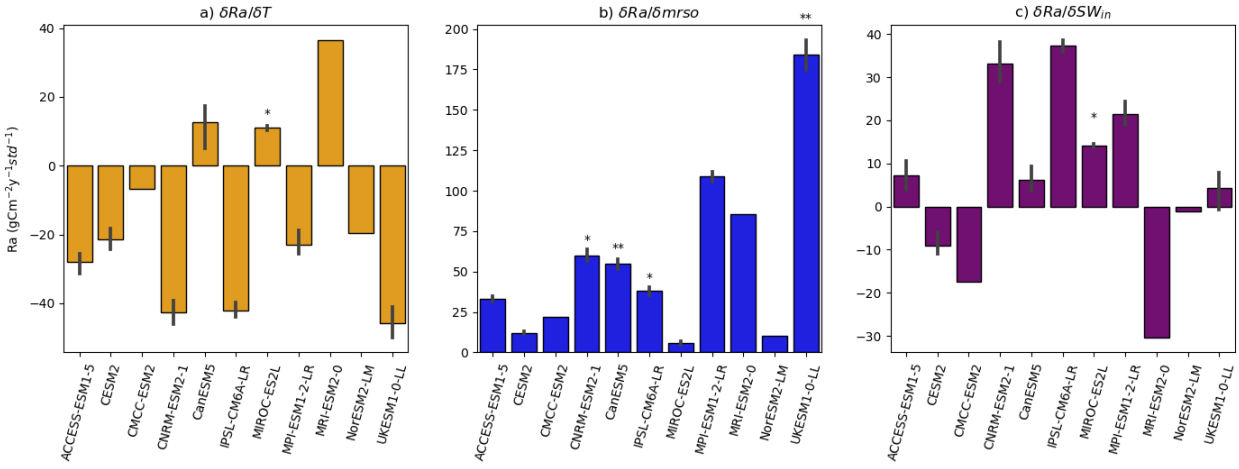

Figure S16: Partial derivatives explaining the contribution of temperature (a), soil moisture (b) and shortwave incoming radiation (c) to interannual Ra, averaged across the Amazon basin. The black vertical bars represent the spread in the predictors coefficients for models with more than one realization available, whereas the stars indicate the level of significance (p-value), averaged over the Amazon basin, associated to every coefficient. Statistical significance refers to the following convention: *: 1.00e-02 < p <= 5.00e-02; **: 1.00e-03 < p <= 1.00e-02; ***: 1.00e-04 < p <= 1.00e-03; ****: p <= 1.00e-04.

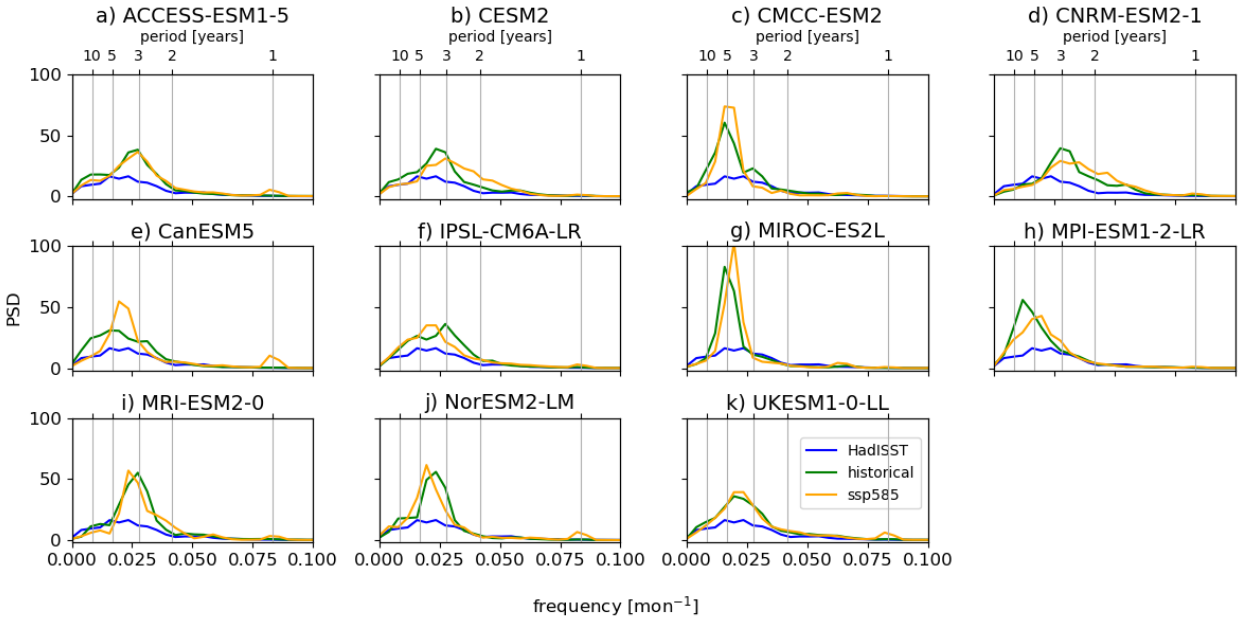

Figure S17: Power Spectrum Density (PSD) of the Nino3.4 signal in all the considered CMIP6 models under the historical (green) and ssp585 (yellow) scenarios. The historical HadISST Nino3.4 frequency (blue line) is added as reference.

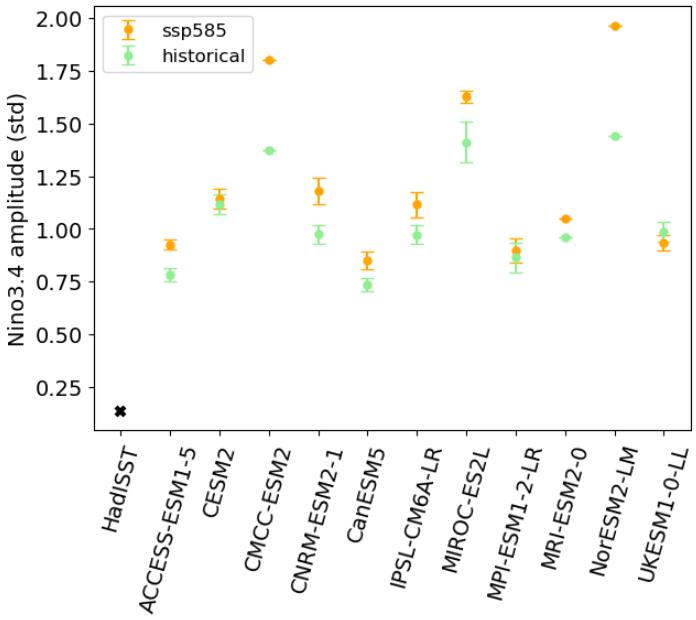

Figure S18: ENSO amplitude change as represented by the Nino3.4 signal standard deviation from the historical period (green crosses) to the future ssp585 scenario (orange dots). The black cross represents the value of Nino3.4 signal amplitude calculated from the HadISST dataset.

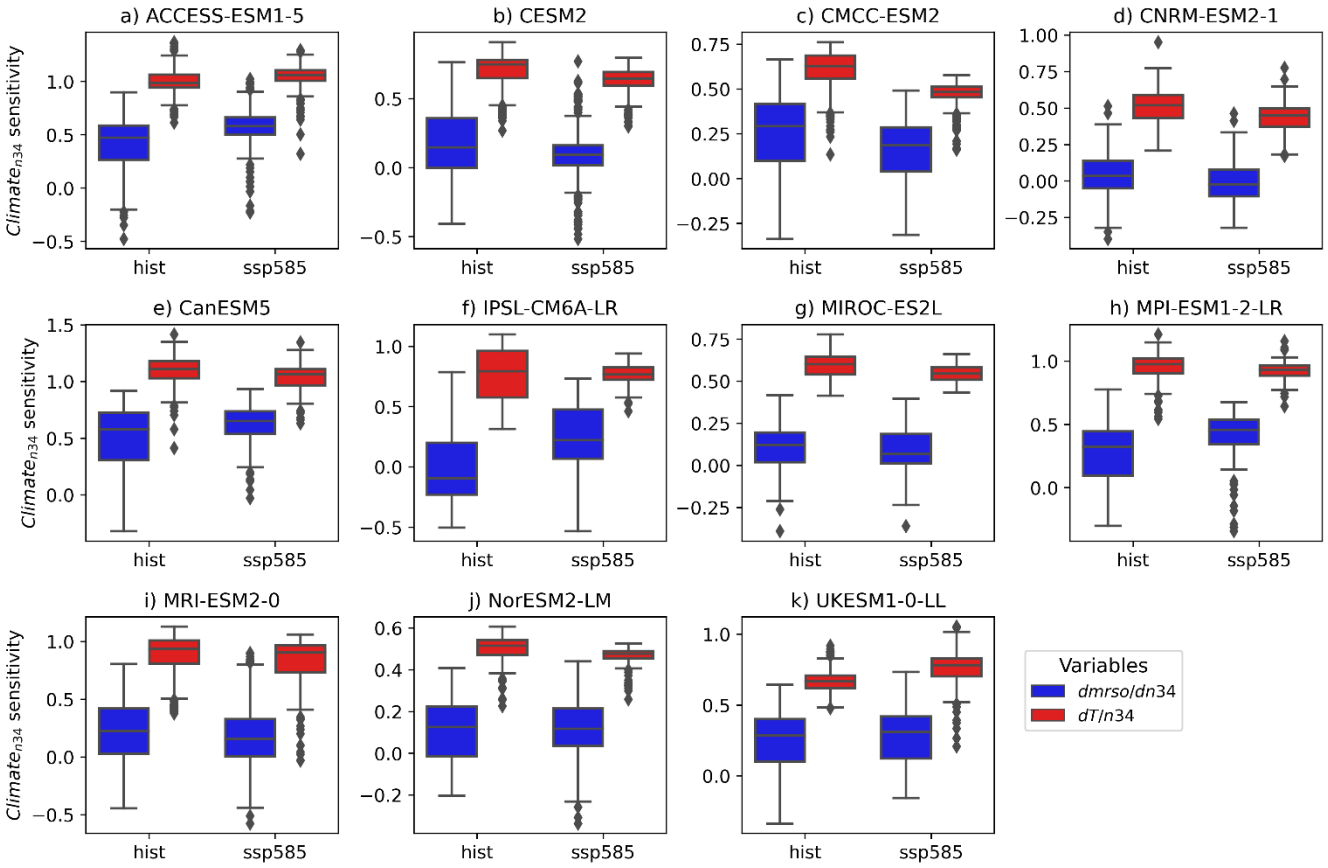

Figure S19: ENSO influence on interannual variability of soil moisture (blue) and temperature (red), for the ESMs considered. Reported are the distribution of univariate coefficients values, masked within the Amazon basin, for both the historical and ssp585 simulations (x-axis).

References

Boucher, O., Servonnat, J., Albright, A. L., Aumont, O., Balkanski, Y., Bastrikov, V., Bekki, S., Bonnet, R., Bony, S., and Bopp, L.: Presentation and evaluation of the IPSL-CM6A-LR climate model, Journal of Advances in Modeling Earth Systems, 12, e2019MS002010, 2020.

Danabasoglu, G., Lamarque, J.-F., Bacmeister, J., Bailey, D. A., DuVivier, A. K., Edwards, J., Emmons, L. K., Fasullo, J., Garcia, R., and Gettelman, A.: The community earth system model version 2 (CESM2), Journal of Advances in Modeling Earth Systems, 12, e2019MS001916, 2020.

Hajima, T., Watanabe, M., Yamamoto, A., Tatebe, H., Noguchi, M. A., Abe, M., Ohgaito, R., Ito, A., Yamazaki, D., and Okajima, H.: Development of the MIROC-ES2L Earth system model and the evaluation of biogeochemical processes and feedbacks, Geoscientific Model Development, 13, 2197–2244, 2020.

Jung, M., Koirala, S., Weber, U., Ichii, K., Gans, F., Camps-Valls, G., Papale, D., Schwalm, C., Tramontana, G., and Reichstein, M.: The FLUXCOM ensemble of global land-atmosphere energy fluxes, Scientific data, 6, 1–14, 2019.

Jung, M., Schwalm, C., Migliavacca, M., Walther, S., Camps-Valls, G., Koirala, S., Anthoni, P., Besnard, S., Bodesheim, P., Carvalhais, N., Chevallier, F., Gans, F., Goll, D. S., Haverd, V., Köhler, P., Ichii, K., Jain, A. K., Liu, J., Lombardozzi, D., Nabel, J. E. M. S., Nelson, J. A., O'sullivan, M., Pallandt, M., Papale, D., Peters, W., Pongratz, J., Rödenbeck, C., Sitch, S., Tramontana, G., Walker, A., Weber, U., and Reichstein, M.: Scaling carbon fluxes from eddy covariance sites to globe: synthesis and evaluation of the FLUXCOM approach, Biogeosciences, 17, 1343–1365, https://doi.org/10.5194/bg-17-1343-2020, 2020.

Lovato, T., Peano, D., Butenschön, M., Materia, S., Iovino, D., Scoccimarro, E., Fogli, P. G., Cherchi, A., Bellucci, A., and Gualdi, S.: CMIP6 Simulations With the CMCC Earth System Model (CMCC-ESM2), Journal of Advances in Modeling Earth Systems, 14, e2021MS002814, 2022.

Mauritsen, T., Bader, J., Becker, T., Behrens, J., Bittner, M., Brokopf, R., Brovkin, V., Claussen, M., Crueger, T., and Esch, M.: Developments in the MPI-M Earth System Model version 1.2 (MPI-ESM1. 2) and its response to increasing CO2, Journal of Advances in Modeling Earth Systems, 11, 998–1038, 2019.

Monteverde, C., De Sales, F., and Jones, C.: Evaluation of the CMIP6 Performance in Simulating Precipitation in the Amazon River Basin, Climate, 10, 122, https://doi.org/10.3390/cli10080122, 2022.

Ortega, G., Arias, P. A., Villegas, J. C., Marquet, P. A., and Nobre, P.: Present-day and future climate over central and South America according to CMIP5/CMIP6 models, International Journal of Climatology, https://doi.org/10.1002/JOC.7221, 2021.

Qiao, L., Zuo, Z., and Xiao, D.: Evaluation of Soil Moisture in CMIP6 Simulations, Journal of Climate, 35, 779–800, https://doi.org/10.1175/JCLI-D-20-0827.1, 2022.

Rayner, N. A. A., Parker, D. E., Horton, E. B., Folland, C. K., Alexander, L. V., Rowell, D. P., Kent, E. C., and Kaplan, A.: Global analyses of sea surface temperature, sea ice, and night marine air temperature since the late nineteenth century, Journal of Geophysical Research: Atmospheres, 108, 2003.

Séférian, R., Nabat, P., Michou, M., Saint-Martin, D., Voldoire, A., Colin, J., Decharme, B., Delire, C., Berthet, S., and Chevallier, M.: Evaluation of CNRM earth system model, CNRM-ESM2-1: Role of earth system processes in present-day and future climate, Journal of Advances in Modeling Earth Systems, 11, 4182–4227, 2019.

Seland, Ø., Bentsen, M., Olivié, D., Toniazzo, T., Gjermundsen, A., Graff, L. S., Debernard, J. B., Gupta, A. K., He, Y.-C., and Kirkevåg, A.: Overview of the Norwegian Earth System Model (NorESM2) and key climate response of CMIP6 DECK, historical, and scenario simulations, Geoscientific Model Development, 13, 6165–6200, 2020.

Sellar, A. A., Jones, C. G., Mulcahy, J. P., Tang, Y., Yool, A., Wiltshire, A., O'connor, F. M., Stringer, M., Hill, R., and Palmieri, J.: UKESM1: Description and evaluation of the UK Earth System Model, Journal of Advances in Modeling Earth Systems, 11, 4513–4558, 2019.

Swart, N. C., Cole, J. N., Kharin, V. V., Lazare, M., Scinocca, J. F., Gillett, N. P., Anstey, J., Arora, V., Christian, J. R., and Hanna, S.: The Canadian earth system model version 5 (CanESM5. 0.3), Geoscientific Model Development, 12, 4823–4873, 2019.

Wild, M., Folini, D., Hakuba, M. Z., Schär, C., Seneviratne, S. I., Kato, S., Rutan, D., Ammann, C., Wood, E. F., and König-Langlo, G.: The energy balance over land and oceans: an assessment based on direct observations and CMIP5 climate models, Clim Dyn, 44, 3393–3429, https://doi.org/10.1007/s00382-014-2430-z, 2015.

Yukimoto, S., Kawai, H., Koshiro, T., Oshima, N., Yoshida, K., Urakawa, S., Tsujino, H., Deushi, M., Tanaka, T., Hosaka, M., Yabu, S., Yoshimura, H., Shindo, E., Mizuta, R., Obata, A., Adachi, Y., and Ishii, M.: The Meteorological Research Institute Earth System Model Version 2.0, MRI-ESM2.0: Description and Basic Evaluation of the Physical Component, Journal of the Meteorological Society of Japan. Ser. II, 97, 931–965, https://doi.org/10.2151/jmsj.2019-051, 2019.

Ziehn, T., Chamberlain, M. A., Law, R. M., Lenton, A., Bodman, R. W., Dix, M., Stevens, L., Wang, Y.-P., and Srbinovsky, J.: The Australian earth system model: ACCESS-ESM1. 5, Journal of Southern Hemisphere Earth Systems Science, 70, 193–214, 2020.